Applications of Concatenated Composite Pulses to NMR

Masamitsu Bando[a], Tsubasa Ichikawa[b], Yasushi Kondo[c,d], Nobuaki Nemoto[e], Mikio Nakahara[c,d], Yutaka Shikano[f,g,h]

[a]*Kinki University Technical College, 7-1 Kasugaoaka, Nabari, Mie 518-0459, Japan*
[b]*Department of Physics, Gakushuin University, 1-5-1 Mejiro, Toshima-ku, Tokyo 171-8588, Japan*
[c]*Research Center for Quantum Computing, Interdisciplinary Graduate School of Science and Engineering, Kinki University, 3-4-1 Kowakae, Higashi-Osaka, Osaka 577-8502, Japan*
[d]*Department of Physics, Kinki University, 3-4-1 Kowakae, Higashi-Osaka, Osaka 577-8502, Japan*
[e]*JEOL RESONANCE Inc., 3-1-2 Musashino, Akishima, Tokyo, 196-8558, Japan*
[f]*Research Center of Integrative Molecular Systems (CIMoS), Institute for Molecular Science, 38 Nishigo-Naka, Myodaiji, Okazaki 444-8585, Japan*
[g]*Institute for Quantum Studies, Chapman University, 1 University Dr., Orange, CA 92866, USA*
[h]*Materials and Structures Laboratory, Tokyo Institute of Technology, 4259 Nagatsuta-cho, Midori-ku, Yokohama, Kanagawa, 226-8503, Japan*

Abstract

ConCatenated Composite Pulses (CCCPs) are derived from various composite pulses widely employed in NMR and have been developed as high-precision unitary operations in Quantum Information Processing (QIP). CCCPs are robust against two systematic errors, pulse-length and off-resonance errors, in NMR simultaneously. We show experiments that demonstrate CCCPs are powerful and versatile tools not only in QIP but also in NMR measurements.

Keywords: Composite pulse, Pulse design

1. Introduction

Nuclear Magnetic Resonance (NMR) is widely employed from Magnetic Resonance Imaging (MRI) in hospitals to precision chemical analysis of various molecules in pharmaceutical companies [1] thanks to highly developed NMR techniques. Some of these advanced techniques in NMR have been transferred to Quantum Information Processing (QIP) [2] since NMR manipulations are regarded as controlling and measuring quantum objects, called spins.

We have been working on transferring one of existing NMR techniques, a composite pulse [3, 4, 5, 6], to QIP and developed high-precision unitary operations [7]. These operations are called ConCatenated Composite Pulses (CCCPs) and are robust against two systematic errors simultaneously at the cost of operation time, namely, the total length of pulses. These errors correspond to pulse-length errors (PLE) and off-resonance errors (ORE) in NMR manipulations. Instead of composing such pulses from scratch, CCCPs are designed by concatenating two composite pulses with different characteristics against systematic errors. Thus these are descendants of existing composite pulses widely employed in NMR. QIP requires high-precision control of spins. Therefore, once CCCPs developed in QIP are employed for NMR measurements, significant improvement of signal strength is expected without any changes in the hardware settings.

Email addresses: bando@ktc.ac.jp (Masamitsu Bando), tsubasa@qo.phys.gakushuin.ac.jp (Tsubasa Ichikawa), ykondo@kindai.ac.jp (Yasushi Kondo), nnemoto@jeol.co.jp (Nobuaki Nemoto), nakahara@math.kindai.ac.jp (Mikio Nakahara), yshikano@ims.ac.jp (Yutaka Shikano)

The purpose of this paper is to feedback our achievement obtained in QIP to NMR measurements. In Sec. 2, we review the idea and properties of CCCPs. Section 3 is the main part of this paper, where the superiority of CCCPs over the conventional methods in NMR measurements, single pulses and COSY, are demonstrated experimentally. Section 4 is devoted to summary and discussions. Some theoretical details are described with simulations in Appendix.

2. Concatenated composite pulse (CCCP)

In this section, we summarize the principle of CCCPs, i.e., composite pulses simultaneously robust against two typical systematic errors, PLE and ORE, in NMR [5].

2.1. Pulse length errors (PLEs) and off-resonance errors (OREs)

The system we consider throughout this paper is a nucleus with spin 1/2 (in short, a *spin*) in a static magnetic field along the *z*-axis. We consider a rotation operation of the spin

$$R(\theta, \phi) = \exp[-\mathrm{i}\theta \boldsymbol{n}(\phi) \cdot \boldsymbol{\sigma}/2] \qquad (1)$$

without errors. θ is the rotation angle, $\boldsymbol{n}(\phi) = (\cos\phi, \sin\phi, 0)$ is the rotation axis in the *xy*-plane, and $\boldsymbol{\sigma} = (\sigma_x, \sigma_y, \sigma_z)$ are the Pauli matrices. This rotation is generated by an ideal rf pulse in NMR.

We consider a realistic square pulse in which both PLE and ORE are present simultaneously. We ignore the second and higher order error terms for simplicity. The rotation associated with a square pulse under only PLE is given as

$$
\begin{aligned}
R'_\varepsilon(\theta, \phi) &= \exp[-\mathrm{i}(1+\varepsilon)\theta \boldsymbol{n} \cdot \boldsymbol{\sigma}/2] \\
&= R(\theta, \phi) - \mathrm{i}\varepsilon\theta(\boldsymbol{n} \cdot \boldsymbol{\sigma})R(\theta, \phi)/2, \qquad (2)
\end{aligned}
$$

where ε is the strength of PLE, which is unknown but we assume that it is constant and small. Higer order terms beyond first order in ε are suppressed in the second equality. This type of errors often appear because of inhomogeneity in the B_1 field or lack of long term stability of spectrometers. On the other hand, the rotation associated with a square pulse under only ORE is given as

$$
\begin{aligned}
R'_f(\theta, \phi) &= \exp[-\mathrm{i}\theta(\boldsymbol{n} \cdot \boldsymbol{\sigma} + f\sigma_z)/2] \\
&= R(\theta, \phi) - \mathrm{i}f \sin(\theta/2)\sigma_z, \quad (3)
\end{aligned}
$$

where f is the strength of ORE. ORE is caused whenever the resonance of interest is not in resonance with the carrier frequency (transmitter frequency). In other words, ORE appears whenever there is a frequency offset between the carrier frequency and the Larmor frequency. Similarly to PLE, f is unknown but we assumed that it is constant and small. Therefore, when both PLE and ORE are present, the rotation associated with a square pulse is given as

$$
\begin{aligned}
&R'(\theta, \phi) \\
&= \exp[-\mathrm{i}(1+\varepsilon)\theta(\boldsymbol{n} \cdot \boldsymbol{\sigma} + f\sigma_z)/2] \\
&= R(\theta, \phi) - \mathrm{i}\varepsilon\theta(\boldsymbol{n} \cdot \boldsymbol{\sigma})R(\theta, \phi)/2 - \mathrm{i}f \sin(\theta/2)\sigma_z. \quad (4)
\end{aligned}
$$

2.2. Composite pulses

The NMR community has been developing a technique to overcome PLE and ORE by combining several pulses [2, 5, 6]. Given a target rotation $R(\theta, \phi)$, we may find an equivalent rotation sequence which is equal to the target $R(\theta, \phi)$ in case of no errors, as follows.

$$
R(\theta_N, \phi_N)R(\theta_{N-1}, \phi_{N-1})\cdots R(\theta_1, \phi_1) = R(\theta, \phi). \quad (5)
$$

Here, $R(\theta_i, \phi_i)$ is the i-th rotation associated with the i-th square pulse and N denotes the number of square pulses. The point of the decomposition (5) is

$$
R'(\theta_N, \phi_N)R'(\theta_{N-1}, \phi_{N-1})\cdots R'(\theta_1, \phi_1) \neq R'(\theta, \phi)
$$

if PLE and/or ORE exist. This is due to the non-commutativity among $R(\theta_i, \phi_i)$. Therefore, by appropriate tuning of the parameters $\{\theta_i, \phi_i\}_{i=1}^N$ in Eq. (5), we can obtain the sequence which i) virtually works as the target $R(\theta, \phi)$ when there are no errors, and ii) is less sensitive to the systematic errors. Indeed, such pulse sequences have been designed [3, 4, 5, 8, 9, 10, 11] by choosing the parameters $\{\theta_i, \phi_i\}_{i=1}^N$ in such a way that Eq. (5) has no first order terms with respect to the error parameter ε or f. Note that these are the type A composite pulses, for which the first order cancellation applies independently of the initial state [5].

Now we present two typical composite pulses that are robust against either PLE or ORE: one is the Broad Band 1 (BB1) [8] and the other is the Compensation for Off-Resonance with a Pulse SEquence (CORPSE) [9]. See, also Appendix A. BB1 under both PLE and ORE behaves as

$$
R'_{\mathrm{BB1}}(\theta, \phi) = R(\theta, \phi) - \mathrm{i}f \sin(\theta/2)\sigma_z. \quad (6)
$$

BB1 is obviously robust against PLE, but not against ORE. Moreover, the first order error term of BB1 is exactly the same
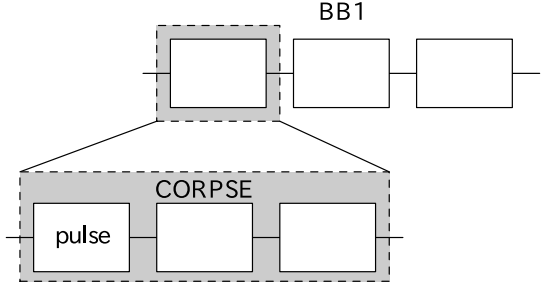

Figure 1: Schematic diagram of CCCP by using BB1 and CORPSE. Time goes from left to right in this pulse diagrams.

as that in Eq. (3). We call the property residual error preserving property (REPP) with respect to ORE.

In contrast to BB1, CORPSE is an $N = 3$ composite pulse robust against ORE. CORPSE behaves as

$$
R'_{\mathrm{CORPSE}}(\theta, \phi) = R(\theta, \phi) - \mathrm{i}\varepsilon(\boldsymbol{n} \cdot \boldsymbol{\sigma})R(\theta, \phi)/2. \quad (7)
$$

CORPSE possesses REPP with respect to PLE.

We pointed out that not all the composite pulses have REPP [13].

2.3. Concatenated composite pulses (CCCPs)

We show how to design a CCCP compensating both PLE and ORE simultaneously by taking the advantage of REPP with BB1 and CORPSE, as an example [12, 13]. BB1 is robust against PLE, while CORPSE is robust against ORE and has REPP with respect to PLE. Therefore, we replace all square pulses in BB1 with CORPSE (see Fig. 1). This CCCP is called CORPSE in BB1, or CinBB in short. The number of square pulses in CinBB is $4 \times 3 = 12$. The number of square pulses in CinBB can be further reduced to $N = 6$ and the resulting CCCP is called the reduced CinBB, or R-CinBB for short. See Appendix A and [13] for further details.

Other interesting approach to tackle both PLE and ORE was discussed by Jones [14]. He designed composite pulses compensating for higher order error terms of both PLE and ORE simultaneously. The rotation angle θ is, however, fixed to π in these composite pulses. For the recent progress of the composite pulses including CCCPs, see the review by Merrill and Brown [15].

3. Advantages of CCCP

The advantages of CCCPs in NMR experiments are demonstrated with various experiments. We employ an ECA-500 NMR spectrometer (JEOL RESONANCE Inc.). We evaluate the performance of the R-CinBB composite pulse as an example and compare the result with that of a square pulse.

3.1. Single Pulses

The experiments are carried out using ^{13}C-labeled chloroform (Cambridge Isotopes) diluted in d_6-acetone of approximately 300 mM concentration at room temperature. In order to shorten T_1 for a rapid repetition, a relaxation agent (4 mM of
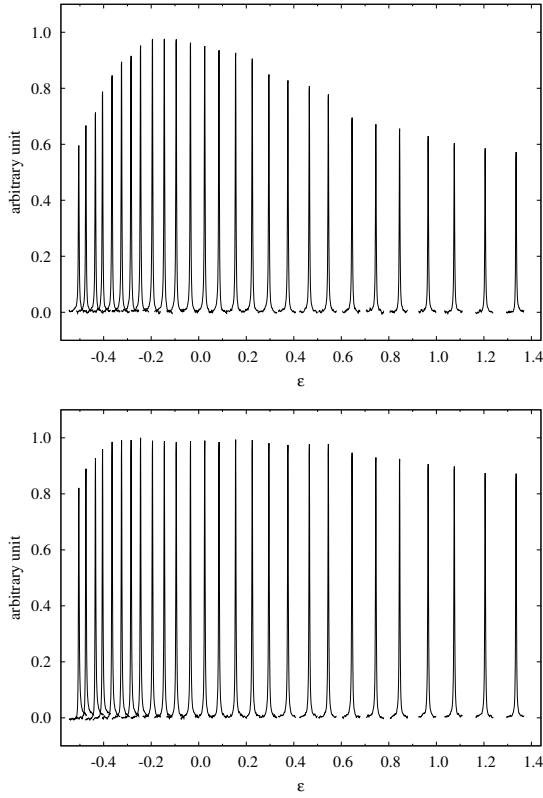
Figure 2: Spectra of FID signals after the $\pi/2$-square pulse (top) and the R-CinBB pulse (bottom) are applied as functions of PLE (ε in Eq. (4)). The strength of ORE is fixed to $f \sim 0$.
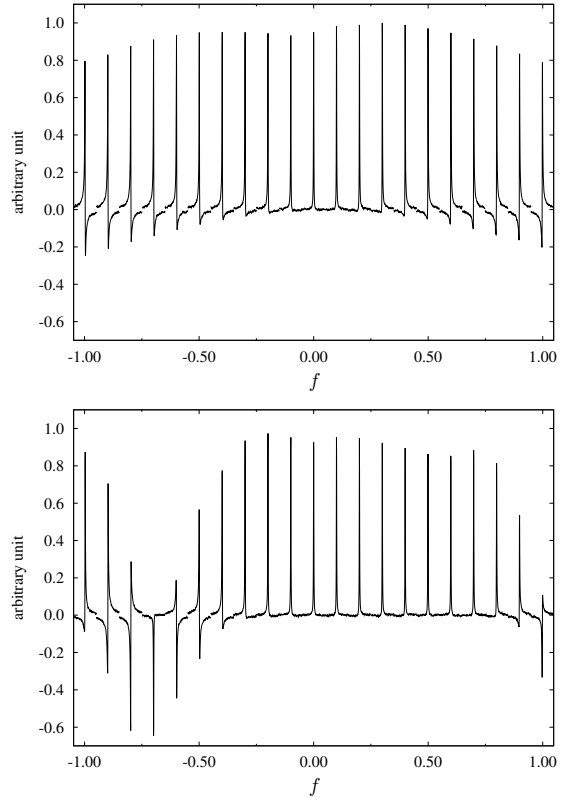

Figure 3: Spectra of FID signals after the $\pi/2$-square pulse (top) and the R-CinBB pulse (bottom) are applied as functions of ORE (f in Eq. 4). The strength of PLE is fixed to $\varepsilon \sim 0$.

Iron(III) acetylacetonate) is added. T_1's and T_2's are $\sim$ 6 s and 200 ms for ^{13}C, respectively, while those of proton are both $\sim$ 200 ms. We examine the performance of a composite $\pi/2$-pulse applied on ^{13}C and compare the result with that of a square pulse while proton is decoupled with WALTZ16 [16].

The determination of the pulse strength is not simple because of inhomogeneity of B_1 in the sample. We take a $\frac{1}{4}$ of the 2π-pulse duration as the nominal pulse duration of a square $\frac{\pi}{2}$ pulse. It is obvious that the R-CinBB composite pulses are more advantageous compared with square pulses in terms of PLE, as shown in Fig 2. See, also numerical calculations shown in Appendix B and [13].

We also examine the R-CinBB composite pulse in terms of ORE, as shown in Fig 3. The R-CinBB composite pulse is obviously more advantageous than the square pulse when $-0.3 < f < 0.8$ in Eq. (4). On the other hand, the spectra of the R-CinBB composite pulses corresponding to $f < -0.5$ and $1.0 < f$ are more distorted than those of the square pulses. See, also numerical calculations shown in Appendix B and the reference [13].

3.2. COSY

The two dimensional shift-COrrelation SpectroscopY (COSY) is one of the most important 2D-NMR measure-

ments [1]. We perform COSY experiments with 3-chloro-2,4,5,6-tetrafluoro-benzotrifluoride diluted in d_6-benzen of an about 300 mM concentration. We observe signals of ^{19}F nuclei directly attached to a benzen ring (^{19}Fs at 2, 4, 5, and 6). T_1's are between 0.6 and 1.0 s, while T_2's are $\sim$ 0.3 s. We use this molecule because of the following reasons. Firstly, as shown in Fig. 4, ^{19}F signals of the molecule are widely spread. Secondly, the spectrum pattern is not so simple, although its molecular strcture is relatively simple.

The pulse duration of a $\pi/2$-square pulse is 12.4 μs which corresponds to a B_1 strength of 20 kHz in frequency unit. Note that the frequency difference between -160 and -118 ppm is 20 kHz at 470 MHz and is comparable with the strength of B_1. The total duration time of the R-CinBB pulse is $12.4 \times 8 = 99.2$ μs that is almost instantaneous like a square pulse in our experimental time scale and thus the replacement of a square pulse by the R-CinBB one leads no problem. The data are analyzed as follows. For both t_1 and t_2 period, shifted sine-bell window function is multiplied. For t_1, zero-filling is done once. This time-domain data is then Fourier-transformed and phased.

B_1 strength of a $\pi/2$-square pulse in frequency is comparable with the frequency difference between the highest and lowest peaks. Therefore, we expect that COSY experiments with square pulses may have some difficulties. There are attempts with BURP (Band-selective, Uniform Response, Pure Phase)
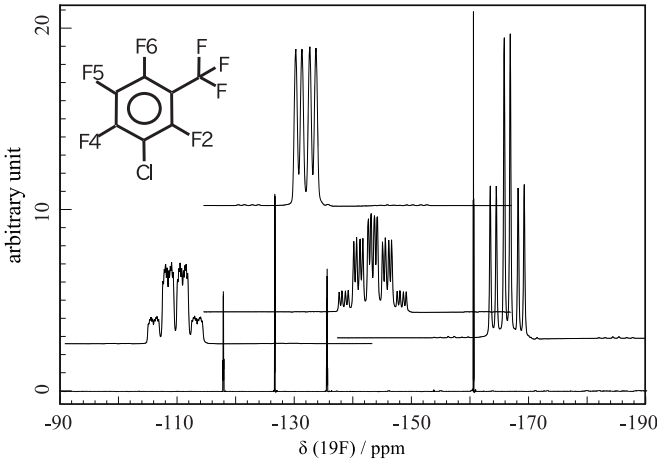
3

Figure 4: ^{19}F spectrum of 3-chloro-2,4,5,6-tetrafluoro-benzotrifluoride ride in d_6-benzen. Each peak is enlarged to show detailed structures (1 ppm). Peak assignments are as follows; 1 (-118.0 ppm), 2 (-126.5 ppm), 3 (-135.5 ppm), and 4 (-160.5 ppm) are identified as F2, F4, F6, and F5, respectively. ^{19}F signal of trifluoromethyl group is not observed in this region.

to overcome these difficulties [17, 18].

As we expected, the correlation peak between -118.0 ppm (f1) and -126.5 ppm (f2), and that between -126.5 ppm (f1) and -118.0 ppm (f2) are hardly visible in the case of square pulses. On the other hand, these are much higher intensities in the case of R-CinBB pulses, although they are small as is found in Fig. 5. The advantage of R-CinBB pulses are more clearly demonstrated in 1-D spectra, as shown in Fig. 6. The phases of peaks obtained with square pulses are highly distorted and this may be the reason why the above correlation peaks are hardly visible.

4. Summary

Composite pulses have been developed in the NMR community and are widely employed in daily measurements. Concatenated composite pulses (CCCPs) are directly descended from them and have been developed as robust unitary operations for quantum information processing. They are robust against two systematic errors, the pulse length error and off-resonance error in NMR, at the cost of execution times. Note, however, that this cost is not important in usual experimental conditions of liquid-state NMR and thus CCCPs are always advantageous compared with square pulses.
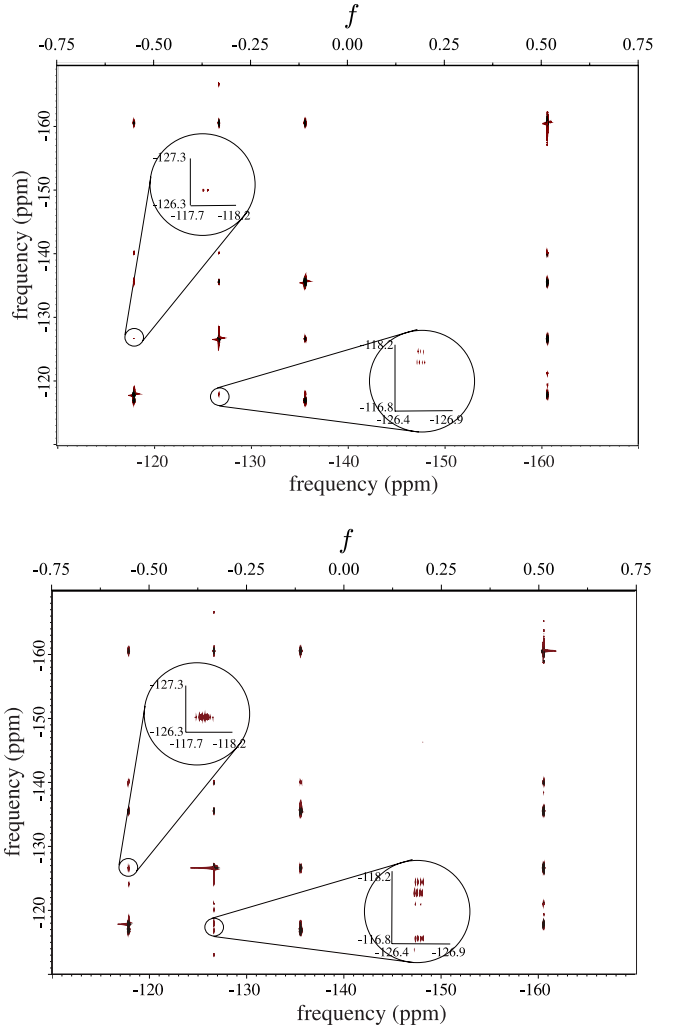
Acknowledgment

Figure 5: 2D-spectra obtained with (a) a square and (b) an R-CinBB pulses.

Appendix A. Example of composite pulses

We present details of the Broad Band 1 (BB1) [8], the Compensation for Off-Resonance with a Pulse SEquence (CORPSE) [9] and the reduced CORPSE in BB1 (R-CinBB) [13].

Appendix A.1. BB1

BB1 is an $N = 4$ composite pulse robust against PLE. The parameters are chosen as

$$\theta_1 = \theta_3 = \pi, \ \theta_2 = 2\pi, \ \theta_4 = \theta,$$
$$\phi_1 = \phi_3 = \phi + \arccos[-\theta/(4\pi)], \ \phi_2 = 3\phi_1 - 2\phi, \ \phi_4 = \phi. \tag{A.1}$$

BB1 under both PLE and ORE behaves as

$$R'_{\mathrm{BB1}}(\theta, \phi) = R'(\theta, \phi)R'(\pi, \phi_1)R'(2\pi, \phi_2)R'(\pi, \phi_1)$$
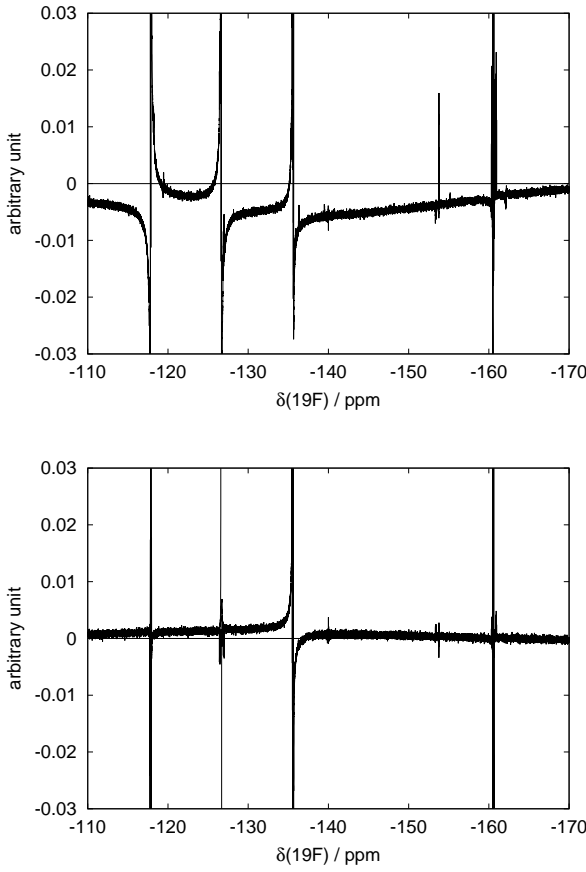$$= R(\theta, \phi) - \mathrm{i}f \sin(\theta/2)\sigma_z. \tag{A.2}$$

4

Figure 6: 1D-spectra obtained with (a) square and (b) R-CinBB pulses in COSY measurements.

Appendix A.2. CORPSE

CORPSE is an $N = 3$ composite pulse robust against ORE. Its parameters are

$$\theta_1 = 2n_1\pi + \theta/2 - k, \ \theta_2 = 2n_2\pi - 2k, \ \theta_3 = 2n_3\pi + \theta/2 - k,$$
$$\phi_1 = \phi_2 - \pi = \phi_3 = \phi, \ k = \arcsin[\sin(\theta/2)/2], \quad (A.3)$$

where n_1, n_2, n_3 are non-negative integers. In particular, when we take $n_1 = n_3 = 0$ and $n_2 = 1$, the execution time is minimized. Then CORPSE is called short CORPSE. Other notable case takes place when $n_1 - n_2 + n_3 = 0$. In this case with both PLE and ORE, CORPSE behaves as

$$R'_{\text{CORPSE}}(\theta, \phi) = R'(\theta_3, \phi)R'(\theta_2, \phi + \pi)R'(\theta_1, \phi)$$
$$= R(\theta, \phi) - i\varepsilon(\boldsymbol{n} \cdot \boldsymbol{\sigma})R(\theta, \phi)/2. \quad (A.4)$$

Appendix A.3. reduced CORPSE in BB1

The R-CinBB is given as follows.

$$\theta_1 = \theta_3 = \pi, \ \theta_2 = 2\pi,$$
$$\theta_4 = \theta_6 + 2\pi = 2\pi + \theta/2 - k, \ \theta_5 = 2\pi - 2k,$$
$$\phi_1 = \phi_3 = \phi + \arccos[-\theta/(4\pi)], \ \phi_2 = 3\phi_1 - 2\phi,$$
$$\phi_4 = \phi_5 - \pi = \phi_6 = \phi, \ k = \arcsin[\sin(\theta/2)/2]. \quad (A.5)$$

For instance, the sequence implements π-pulse when

$$\theta_1 = \theta_3 = \phi_5 = \pi, \ \theta_2 = 2\pi,$$
$$\theta_4 = 7\pi/3, \ \theta_5 = 5\pi/3, \ \theta_6 = \pi/3,$$
$$\phi_1 = \phi_3 = \pi - \arccos(1/4), \ \phi_2 = 3\phi_1,$$
$$\phi_4 = \phi_6 = 0. \quad (A.6)$$

Appendix B. Simulations of NMR experiments

We perform some numerical simulations in order to support experiments.

Appendix B.1. method

We have to take into account of a non-unitary time development caused by a spin-spin relaxation with a characteristic time T_2, in order to simulate NMR experiments. We introduce this effect as a phase flip channel [19].

In the case of single spin experiments,

$$\rho(t + \Delta) = p_{ss}(\Delta)\rho(t) + (1 - p_{ss}(\Delta))\,\text{Ad}\,(\sigma_z, \rho(t)),$$
$$p_{ss}(\Delta) = \frac{1 + \exp(-\Delta/T_2)}{2},$$

where $\text{Ad}(*, \rho) = *\rho*^\dagger$ and Δ is a small time interval.

During a pulse, the time evolution is simulated as follows.

$$\rho'(t + \tau_p) = p_{ss}(\tau_p)\rho(t) + \left(1 - p_{ss}(\tau_p)\right)\text{Ad}\,(\sigma_z, \rho(t)),$$
$$\rho(t + \tau_p) = \text{Ad}(U_{\text{pulse}}, \rho'(t + \tau_p)),$$

where U_{pulse} is a unitary operation generated by the pulse. Note that τ_p is the total pulse duration and is assumed to be small. Therefore, we employ the Suzuki-Trotter formula [20], here.

In the case of COSY experiments, the simulations during the evolution and detection periods [1] are done as follows.

$$\rho'(t + \delta) = \left(1 - \frac{\delta}{2T_{2,1}} - \frac{\delta}{2T_{2,2}}\right)\rho(t)$$
$$+ \frac{\delta}{2T_{2,1}}\text{Ad}(\sigma_z \otimes \sigma_0, \rho(t))$$
$$+ \frac{\delta}{2T_{2,2}}\text{Ad}(\sigma_0 \otimes \sigma_z, \rho(t)),$$
$$\rho(t + \delta) = \text{Ad}(\exp(-J\delta\frac{\sigma_z \otimes \sigma_z}{4}), \rho'(t + \delta)),$$

where $T_{2,i}$ is the T_2 of the i-th spin. $\rho(t + n\delta)$ can be obtained by iterating the above operations n-times. We assume that the scalar coupling is in a weak coupling limit [21]. Note that the above decomposition is based on the Suzuki-Trotter formula [20] by assuming δ is sufficiently small and that $p_{ss}(\delta) \approx 1 - \delta/(2T_{2,i})$ for the i-th spin.

During a pulse, the time development is similarly simulated as in the case of single spin experiments.

Appendix B.2. Single pulses

The signal amplitude is estimated in the case of a typical NMR measurement where a control field (B_1 in NMR) is inhomogeneous over the sample and assumed to have the Gaussian distribution [22].

$$p(B_1) = \frac{1}{\sqrt{2\pi}\sigma} \exp\left[-\frac{(B_1 - \bar{B}_1)^2}{2\sigma^2}\right], \qquad (B.1)$$

where $\bar{B}_1$ is the average strength of B_1 and σ determines the inhomogeneity. On this assumption with a previously estimated value of $\sigma = 0.05$ [22] with our NMR spectrometer, the signal strength distributions after a nominal $\pi/2$-pulse (or, $\bar{B}_1 \tau_p = \pi/2$ where τ_p is the pulse duration) is calculated, as shown in Fig. B.7. It is obvious that R-CinBB is advantageous over the square pulse.
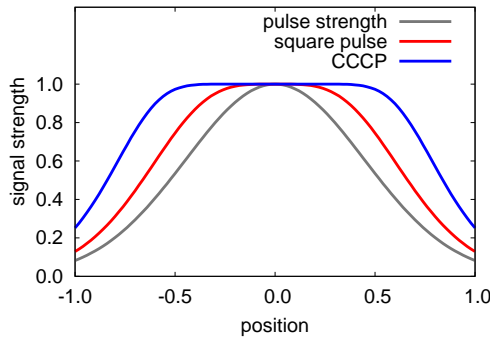

Figure B.7: (colour online) Projection of magnetization on the *xy*-plane after a pi/2-pulse. The red (blue) curve is the outcome of a square pulse (the R-CinBB pulse) as a function of *z* along the sample. The gray line indicates the strength of B_1 as a function of *z*.

A phase error in the NMR spectrum occurs under ORE, as shown in Fig. B.8. Here, $f = 0.1$ is assumed. The red curve in this figure is a simulated result of a square $\pi/2$-pulse and appears distorted. On the other hand, the blue curve is a simulated result of a R-CinBB-$\pi/2$-pulse and is not distorted.
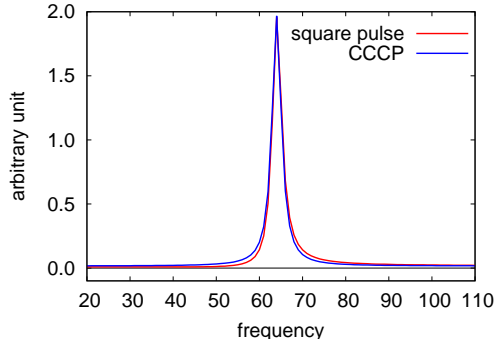

Figure B.8: (colour online) Simulated NMR spectra under ORE. The red curve is a simulated result of the square $\pi/2$-pulse with $f = 0.1$ and appears distorted. On the other hand, the blue curve is a simulated result of R-CinBB pulse with the same f and is not distorted.

Appendix B.3. Hahn echo

Two pulses in Hahn echo experiments [21] are affected by PLE and ORE, thus measured T_2 under such errors may be erroneous. We simulate an NMR equipment with fluctuating PLE and ORE by varying PLE and ORE in every spin echo measurement, as shown in Fig. B.9. Their means are $\bar{\varepsilon} = \bar{f} = 0.1$ and their standard deviations are both 0.08. Although these figures may be unreasonably large for modern NMR spectrometers, we can obtain the correct T_2 with R-CinBB pulses.
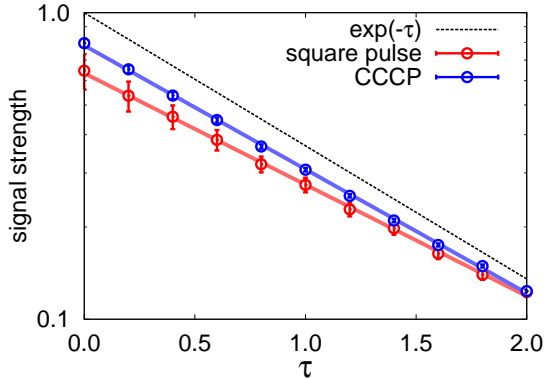

Figure B.9: (colour online) Semi-log plot of echo signal with square pulses (red line) and R-CinBB pulses (blue line) as a function of the waiting time τ. Black dashed line is in error-free case.

Numerical simulations of the Hahn echo experiments as a function of the error strengths are summarized in Fig. B.10. The Hahn echo experiments with square pulses (left figure) are strongly affected by PLE, while those with R-CinBB pulses are robust against these errors. It turns out that a composite pulse robust against PLE is sufficient in order to obtain a correct T_2 under both PLE and ORE.
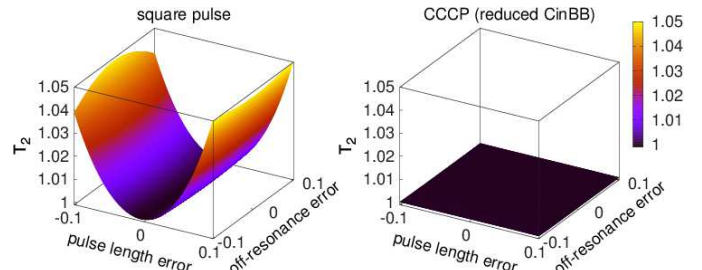

Figure B.10: (colour online) Simulated T_2 with square pulses (left) and with R-CinBB pulses as a function of PLE and ORE. The Hahn echo experiments with R-CinBB pulses give us correct T_2's even in erroneous cases.

Appendix B.4. COSY

Here, we simulate COSY experiments applied for two-spin molecules of which interaction is a scalar coupling in a weak coupling limit, as shown in Fig B.11. The chemical shifts of these spins are assumed to be 1 and 4 ppm and $J = 0.5$ ppm. In COSY experiments, spurious peaks called axial peaks sometimes appear due to inaccuracy of the first pulse [1]. We are able to reproduce these axial peaks in the simulation of COSY experiments with square pulses ($\varepsilon = f = 0.1$), as shown in

Fig. B.11. On the other hand, no axial peaks appear in the simulation with R-CinBB pulses.
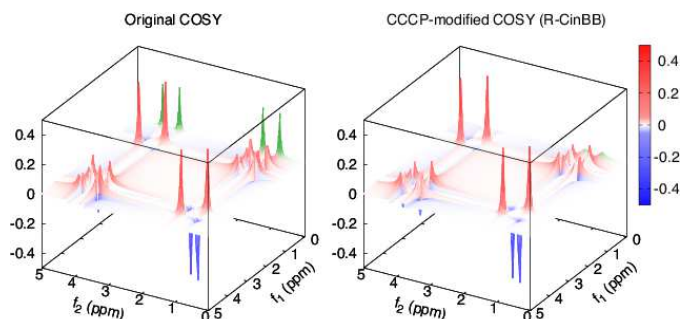

Figure B.11: (colour online) Simulation of COSY experiments of a two-spin molecule with with square pulses (left) and R-CinBB pulses (right), where $\varepsilon = f = 0.1$, $J = 0.5$ ppm and chemical shifts are 1 and 4 ppm. Spurious axial peaks (green peaks) are observed in the simulation with square pulses, while no such peaks are observed in that with R-CinBB pulses.

References

[1] T. D. W. Claridge, "*High-Resolution NMR Techniques in Organic Chemistry*" (Elsevier, Amsterdam, 1999).

[2] J. A. Jones, Prog. Nucl. Magn. Resonance Spectrosc. **59** (2011) 91.

[3] C. Counsell, M. H. Levitt, and R. R. Ernst, J. Magn. Resonance **63** (1985) 133.

[4] R. Tycko, R. A. Pines, and J. Guckenheimer, J. Chem. Phys. **83** (1985) 2775.

[5] M. H. Levitt, Prog. Nucl. Magn. Resonance Spectrosc. **18** (1986) 61.

[6] M. H. Levitt, "Composite pulses" in Encyclopedia of nuclear magnetic resonance, Eds. D. M. Grant and R. K. Harris (Wiley, 1996).

[7] T. Ichikawa, M. Bando, Y. Kondo, and M. Nakahara, Phil. Trans. R. Soc. A **370** (2012) 4671.

[8] S. Wimperis, J. Magn. Resonance A **109** (1994) 221.

[9] H. K. Cummins, G. Llewellyn, and J. A. Jones, Phys. Rev. A **67** (2003) 042308.

[10] K. R. Brown, A. W. Harrow, and I. L. Chuang, Phys. Rev. A **70** (2004) 052318 [Errata **72** (2005) 039905].

[11] W. G. Alway and J. A. Jones, J. Magn. Resonance **189** (2007) 114.

[12] T. Ichikawa, M. Bando, Y. Kondo, and M. Nakahara, Phys. Rev. A **84** (2011) 062311.

[13] M. Bando, T. Ichikawa, Y. Kondo, and M. Nakahara, J. Phys. Soc. Jpn. **82** (2013) 014004.

[14] J. A. Jones, Phys. Rev. A **87** (2013) 052317.

[15] J. T. Merrill and K. R. Brown, in Quantum Information and Computation for Chemistry: Advances in Chemical Physics Volume 154, Ed. S. Kais, (John Wiley and Sons, Inc., Hoboken, New Jersey, 2014).

[16] A. J. Shaka, J. Keeler, and R. Freeman, J. Magn. Reson. **53** (1983) 313.

[17] S. L. Patt, J. Magn. Reson. **96** (1992) 94, S. Cheatham and J. Groce, J. Fluorine Chem. **125** (2004) 1111.

[18] K. Asakura, JEOL News **38** (2006) 20.

[19] M. A. Nielsen and I. C. Chuang, *Quantum Information and Quantum Computation*, (Cambridge University Press, Cambridge, 2000).

[20] M. Suzuki, Phys. Lett. A **165** (1992) 387.

[21] M. H. Levitt, *Spin Dynamics*, (John Wiley and Sons, New York, 2008).

[22] E. H. Lapasar, K. Maruyama, D. Burgarth, T. Takui, Y. Kondo and M. Nakahara, New J. Phys., **14** (2012) 013043.

[23] R. R. Ernst and W. A. Anderson, Rev. Sci. Instrum. **37** (1966) 93.

[24] H. Günther, "*NMR Spectroscopy: Basic Principles, Concepts, and Applications in Chemistry*" third edition (Wiley-VCH, Weinheim, Germany, 2013).